Chemical Physics Impact 8 (2024) 100428

Contents lists available at ScienceDirect

Chemical Physics Impact

journal homepage: www.sciencedirect.com/journal/chemical-physics-impact

Full Length Article

Fluidized bed reactor for 4-chlorophenol photodegradation via solar and visible radiation using ZnO/g-C_3N_4/carbon xerogel as a photocatalyst

Maira Elizabeth Vicente Gouvea [a], Flávio Henrique Covolam Boldrin [a], Bruno Henrique Baena da Silva [a], Livia Kent Paiva [a], Nicolas Perciani de Moraes [b], Leandro Gonçalves de Aguiar [a], Liana Alvares Rodrigues [a,*]

[a] Escola de Engenharia de Lorena-EEL/USP, Estrada Municipal do Campinho S/N, CEP 12602-810, Lorena, São Paulo, Brazil
[b] São Carlos Institute of Chemistry, University of São Paulo, Av. Trab. São Carlense, 400 - Parque Arnold Schimidt, São Carlos - SP, 13566-590

ARTICLE INFO

Keywords:
Zinc oxide
Fluidized bed reactor
Photocatalysis
4-chlorophenol

ABSTRACT

This study investigates the feasibility of employing a fluidized bed reactor for the degradation of 4-chlorophenol (4CP), considering multiple operational parameters (type of radiation, fresh inlet flow rate and recycle flow rate). The selection of the ZnO/g-C_3N_4/carbon xerogel as photocatalyst, a choice motivated by the improved charge transfer and increased catalyst activity under visible radiation provided by the presence of carbon xerogel and g-C_3N_4, was previously determined through tests conducted in a jacketed batch reactor under visible radiation, in which the ternary material efficiency was compared to their constituting counterpart materials. The semiconductors constituting the unary, binary, and ternary materials were chosen based on considerations of availability, sustainability, and abundance in nature. The use of the proposed fluidized bed reactor brings advantages in scalability, distribution of irradiated light and overall costs when compared to commonly used batch reactors, whereas the investigation of the flow parameters involved in such process is of great importance to understand and optimize the efficiency of the pollutant degradation process. Regarding the ternary photocatalyst, X-ray diffractometry (XRD) revealed the presence of zinc oxide's hexagonal crystalline structure. Moreover, additional characterization using Raman spectroscopy, Fourier-transform infrared spectroscopy (FT-IR), scanning electron microscopy (SEM), transmission electron microscopy (TEM), and energy-dispersive spectroscopy (EDS) confirmed the presence not only of ZnO but also of carbon xerogel and g-C_3N_4 in the composite. From the photodegradation experiments, it was determined that the optimal fresh inlet flow rate to achieve the best degradation, as well as the recycle flow rate for this purpose, were 0.07 and 25 L h^{-1}, respectively. Mathematical simulations described that the model that best fits the system's behavior considers the specific reaction rate as dependent on the concentration of the catalyst in the medium.

1. Introduction

Recently, environmental pollution and water bodies' contamination have emerged as some of the key topics of interest in the extensive discussion of global environmental issues [1,2]. A variety of pollutants, such as heavy metals, personal care products, pesticides, and dyes, have been found in quantities varying from nanograms per liter (ng L^{-1}) to micrograms per liter (μg L^{-1}) in natural water bodies, falling into the class known as Emerging Pollutants (EPs) [1–5]. At these concentrations, EPs may lead to the propagation of several ecological disturbances, such as bioaccumulation in living organisms, microbial resistance, and genetic mutations in mammals [4,6].

4-chlorophenol (4CP), a commonly used pesticide, belongs to the class of chlorophenols and is seen as a representative EP due to its presence in effluents from various industries, ranging from pharmaceutical to petrochemical facilities [6,7]. Its high toxicity, coupled with its potential carcinogenicity, has led it to be listed as one of the priority pollutants by the US Environmental Protection Agency and European Decision 2455/2001/EC [6,8,9]. Therefore, the search for efficient techniques for the remediation of 4CP in industrial wastewaters is crucial.

In this context, heterogeneous photocatalysis has garnered significant interest, because of its capacity to transform organic pollutants into non-toxic substances (such as CO_2, water, and inorganic salts) making it a green and sustainable technology [1,2,10–12]. Through this advanced

* Corresponding author.
E-mail address: liana.r@usp.br (L.A. Rodrigues).

https://doi.org/10.1016/j.chphi.2023.100428
Received 19 October 2023; Received in revised form 23 November 2023; Accepted 10 December 2023
Available online 12 December 2023

Nomenclature

A	Reactants (4CP)
P	Products
X_A	Conversion of reactants
X_{Ag}	Global conversion
k	Specific reaction rate (h^{-1})
τ	Residence time (h)
F_{A_0}	Reactor fresh inlet flow (mol L^{-1})
F_{A_1}	Reactor total inlet flow (mol L^{-1})
F_{A_2}	Reactor outlet flow (mol L^{-1})
F_{A_R}	Reactor recycle inlet flow (mol L^{-1})
$F_{A_{iR}}$	Recycle tank inlet flow (mol L^{-1})
F_{A_e}	Exit tank inlet flow (mol L^{-1})
t	Time (h)
C_{A_0}	Reactor fresh inlet conc. (mol L^{-1})
C_{A_2}	Reactor outlet conc. (mol L^{-1})
C_{A_R}	Reactor recycle inlet conc. (mol L^{-1})
C_{A_e}	Exit tank conc. (mol L^{-1})
C_{C_R}	Catalyst conc. at recycle tank (mol L^{-1})
C_c	Catalyst conc. at reactor outlet (mol L^{-1})
v_0	Reactor fresh inlet volum. flow (L h^{-1})
v_1	Reactor total inlet volum. flow (L h^{-1})
v_R	Reactor recycle inlet volum. flow (L h^{-1})
V	Reactor volume (L)
V_e	Exit tank volume (L)
N_{A_R}	Mols in the recycle tank (mol)
N_{A_e}	Mols in the exit tank (mol)

oxidation process, the energy obtained from light irradiation at a specific wavelength can be absorbed by a photocatalytic material, leading to the promotion of electrons to the conduction band of the photocatalyst while also inducing the accumulation of electron holes on its valence band. This so-called electron/hole pair may then act toward both the oxidation of water and the reduction of oxygen molecules adsorbed on the photocatalyst, generating active radicals responsible for pollutant degradation [1,10].

Zinc oxide (ZnO) is considered to be one of the primary photocatalysts employed for degradation purposes, offering low cost of production, great availability, and high oxidative capacity [2,13,14]. However, its wide bandgap energy (3.22 eV) results in low absorption of visible light, which in combination with a high electron/hole recombination rate, reduces its viability for application under more industrially relevant light sources (solar and visible) [14–16]. Hence, the combination of ZnO with other semiconductors, through the formation of solid-state heterojunctions, emerges as a good alternative to remediate these issues [14–16]. In this context, graphitic carbon nitride (g-C_3N_4) is a semiconductor characterized by its remarkable stability, cost-effectiveness, and a low bandgap energy [14,17–20]; additionally, this semiconductor is ideally suited for the development of efficient heterojunctions [19,20], especially with ZnO as showed by recent studies [18], facilitating enhanced light absorption in the visible spectrum and minimizing the rate of electron/hole recombination [14]. Moreover, employing carbon xerogel for the formation of a ternary composite can result in enhanced properties toward photocatalytic applications, such as higher electrical conductivity and larger specific surface area, improving charge transfer efficiency and photocatalytic efficiency [16]. Furthermore, for this purpose, the utilization of black wattle tannin as a precursor for the proposed carbon xerogel can reduce costs and environmental impacts [21]. Therefore, the use of the ZnO/g-C_3N_4/carbon xerogel composite system is a promising alternative for EP degradation, as demonstrated in our previous work [22].

However, besides the type of photocatalyst, the reactor used for photocatalytic processes and its operational parameters play a crucial role in the overall photodegradation efficiency. Although studies point to the high photodegradation efficiency in batch systems [23,24], continuous systems for microreactors have garnered recent attention due to several advantages, including better uniformity of light irradiation in the reaction mixture, easier scaling up, and potential reduction in reaction time, minimizing the formation of byproducts [25].

The fluidized bed reactor, in particular, is a continuous reactor based on the fluidization of a catalyst according to the fluid velocity passing through the reactor, maintaining a strong contact between the catalyst and the reactive fluid throughout the process, minimizing mass transfer limitations, and facilitating pH and temperature control, to the point of achieving uniform temperatures [26]. Its use has already been proven successful in a wide range of advanced oxidation processes, and, in addition to the benefits mentioned earlier, the simple and cost-effective nature of such an operational strategy aligns perfectly with the search for more cost-efficient photocatalysis processes [26–28].

Aiming to further improve the viability of photocatalytic processes, the use of computational simulation has been widely employed as an efficient tool to accurately describe and predict the phenomena occurring in a vast array of reactional systems [29–31]. The authors, for example, used mathematical models and numerical integration to better describe the kinetics of pollutant degradation reactions, such as landfill leachate and dairy wastewaters, achieving excellent results compared to experimental data [29–31]. Moreover, computational tools for effluent treatment control have been recently widely studied by laboratories and industries, further stimulating the search for mathematical models that accurately describe degradation processes [30,32].

Thus, this study aims to investigate the feasibility of a fluidized bed reactor for 4-chlorophenol (4CP) degradation using the ternary ZnO/g-C_3N_4/carbon xerogel as a photocatalyst, considering multiple operational parameters (type of radiation, fresh inlet flow rate and recycle flow rate). Furthermore, mathematical modeling and numerical integration methods were used to study the kinetic behavior of the system, striving to better comprehend the behavior of the proposed photocatalytic reactor. A preliminary study preceding the proposed analyses in the continuous system was also conducted, with the aim of assessing the enhanced efficiency of the ternary compound under consideration and its photocatalytic properties.

2. Materials and methods

2.1. Synthesis of the ternary photocatalyst

Firstly, the g-C_3N_4 composite was prepared through the thermal polymerization of urea in a muffle furnace. The temperature of 550°C was used, with a heating rate of 10°C min^{-1}, for 2 hours [22].

The composite ZnO/g-C_3N_4/carbon xerogel (2.5% g-C_3N_4, 97.5% ZnO w/w with addition of 0.25g tannin) was prepared similarly as per one of our previous works [22], but using ethanol as solvent. The preparation starts by dissolving 4.5g of $ZnCl_2$ (97% w/w, Neon Analytic) in 25 mL of 99% w/w ethanol (solution A). Following the full dissolution of $ZnCl_2$, 0.07 g of g-C_3N_4 were introduced into the mixture, and it was subjected to stirring for 10 minutes at room temperature. Then, 1.5 mL of 37% CH_2O (37% w/w, Neon Analytic) and 0.25 g of black wattle tannin (PHENOTAN AP, Tanac S.A.) were mixed into the solution. Another solution (solution B) was prepared by diluting 4 g of KOH (>85% w/w, Neon Analytic) in 25 mL of ethanol. Solution B was added to solution A, causing the composite material to precipitate. The dispersion was stirred for an additional 10 minutes. The resulting material was washed until it reached a pH = 7, and then it was dried in an oven until a constant weight was attained. Subsequently, the material

was sieved (325-mesh sieve) and subjected to calcination in an inert atmosphere at 300ºC for a duration of 30 minutes.

The synthesis of ZnO, ZnO/carbon xerogel, and ZnO/g-C_3N_4 (2,5% g-C_3N_4, 97,5% ZnO w/w) followed the same method, but with some changes in the preparation of solution A: for the production of ZnO, no tannin, formaldehyde or g-C_3N_4 were added; for the ZnO/carbon xerogel, no g-C_3N_4 was added; and for the ZnO/g-C_3N_4, no tannin or formaldehyde were added.

2.2. Photocatalytic properties and mechanism evaluation

Aiming to study and assess the superior activity of the ternary material compared to its unary (ZnO, g-C_3N_4) and binary (ZnO/carbon xerogel, ZnO/ g-C_3N_4) counterparts, degradation tests of 4-chlorophenol (4CP) were conducted in a jacketed batch reactor under visible radiation (Osram Powerstar 400W, with an UV filter) using the mentioned photocatalysts. The use of visible radiation for evaluating the activity of photocatalysts is of interest, given the sensitization provided by the use of carbon xerogel and g-C_3N_4 [33]. 0.1 g of photocatalyst was added to solutions of 4-chlorophenol (0.5 L, 10 mg L^{-1}), and the solutions were kept in the dark until adsorption equilibrium was reached. After reaching equilibrium, the light was turned on, and the experiments were carried out for 300 minutes or until the solution reached a null 4CP concentration, whichever occurred first. Samples were collected every 15 minutes for the first hour and subsequently at 30-minute intervals, then filtered through disposable 0.22 μm filters, and the concentration of 4CP in the filtrate was determined using a Shimadzu UV-2600 spectrophotometer at a characteristic wavelength (224 nm) [16]. Moreover, the degradation efficiency was calculated for each sample, using Equation 1 [34]:

$$Degradation\ (\%): \frac{[4CP]_{initial}\ (mg\ L^{-1}) - [4CP]_{instant}\ (mg\ L^{-1})}{[4CP]_{initial}\ (mg\ L^{-1})} \times 100 \quad (1)$$

Furthermore, electrochemical impedance spectroscopy was performed to better discern the charge transfer behavior of the materials. For this purpose, a quartz single-compartment cell with a three-electrode system was employed, consisting of a rotating platinum disk working electrode, a platinum foil counter electrode, and a saturated Ag/AgCl reference electrode. A 0.1 mol L^{-1} potassium sulfate solution served as the electrolyte in the test, and a PalmSens4 potentiostat was used for the measurements [16,35]. The experiments were conducted under visible radiation.

Moreover, diffuse reflectance spectroscopy analysis was conducted for the ternary system and its unary (ZnO, g-C_3N_4) and binary (ZnO/g-C_3N_4, ZnO/carbon xerogel) counterparts. The acquired data were employed to assess the absorption ranges of the materials, identify their bandgaps and determine the energy levels of the conduction and valence bands for the unary materials. The spectra were obtained using a Shimadzu UV-2600 spectrophotometer equipped with an integrating sphere. The acquisition range spanned from 220 to 700 nm, with barium sulfate used as the reference material.

After confirming the superior efficiency of the ternary material, the degradation efficiency of 4-chlorophenol (4CP) was also assessed under solar radiation (Osram Ultra-Vitalux lamp, 300W) for this photocatalyst in a jacketed batch reactor. The aim of these experiments was to comprehend the behavior of the ternary photocatalyst under a distinct radiation source, which is also of interest, and to facilitate a subsequent comparison with the activity observed in the continuous system, which constitutes the primary focus of this study.

Additionally, to investigate the mechanism of active radical generation of the ternary photocatalyst, experiments similar to those described earlier were conducted in a jacketed batch reactor under solar radiation. However, in these experiments, the following compounds were added to act as scavengers: 0.025 mmol L^{-1} potassium chromate (99% w/w, Synth) as an electron scavenger; 5% v/v isopropanol (99.5% w/w Synth) as a hydroxyl radical scavenger; 0.5 L min^{-1} nitrogen gas as a superoxide scavenger; and 0.5 mmol L^{-1} sodium oxalate (99% w/w, Dinâmica LTDA.) as a vacancy scavenger.

Finally, following optimization and the study of photocatalytic properties, the ternary material (ZnO/g-C_3N_4/carbon xerogel) was employed for the continuous system study.

2.3. Characterization

The ternary material prepared for this study underwent a comprehensive characterization process employing diverse analytical techniques. X-ray diffractometry (XRD) was utilized to identify the crystalline phases within the ternary system. This analysis was executed using a PANalytical Empyrean X-ray diffractometer equipped with CuKα radiation, functioning at 40 kV and 30 mA. The XRD analysis was conducted with a step size of 0.026° and had an acquisition time of 29.07 seconds per step, covering the 2θ range from 20 to 70°.

The morphology of the composite was inspected through both transmission electron microscopy (TEM) and scanning electron microscopy (SEM). Transmission electron micrographs were obtained using a JEOL JEM-2100 microscope, featuring a Gatan 2K digital camera, whereas the scanning electron micrographs were obtained with a TESCAN MIRA 3 microscope. Elemental composition analysis was carried out using energy-dispersive spectroscopy (EDS), for this purpose an Oxford spectrometer model Swift ED3000 coupled with the scanning electron microscope was used.

Furthermore, the ternary chemical structure was characterized through Fourier-transform infrared spectroscopy (FT-IR), utilizing a universal attenuated total reflectance (UATR) accessory on a Perkin Elmer Frontier model spectrometer. These analyses were conducted in the spectral range of 4000 to 450 cm^{-1}, with a resolution of 4 cm^{-1}, comprising 16 scans for each analysis. Finally, the structure of the photocatalyst was examined through Raman scattering spectroscopy, employing a HORIBA LabRAM HR Evolution spectrometer equipped with an optical microscope and a λ=532 nm laser. The Raman spectra were collected within the 200-1800 cm^{-1} range, with an acquisition time of 30 seconds and two scans per sample.

2.4. Continuous reactor system

The reactional system employed in this work consisted of a continuous fluidized bed reactor, as described in Fig. 1. For its construction, a quartz reactor (R1) with a volume of 150 mL and an internal diameter of 2 cm was used. The feed consisted of two tanks: T1 contained the fresh inlet solution with the 4CP pollutant (1000 mL of a solution with 10 mg L^{-1} of 4CP), and T2 contained the recycle solution with an initial 0.2 g of the ternary photocatalyst (a fraction of the already processed solution, returning to the system for reprocessing). In tank T2, a volume of 200 mL of solution was maintained under magnetic stirring for optimal catalyst dispersion. The value of the outlet flow rate from T2 was kept equal to the value of the inlet flow rate to maintain the volume of T2 constant. Two peristaltic pumps were used to control the flows, and silicone hoses were used to promote flow between the described parts, totaling a volume of 50 mL. The source of simulated sunlight (Osram Ultra-Vitalux lamp, 300W) or visible light (Osram Powerstar 400W, with an UV filter) was positioned 10 cm from the reactor in each case. The experiments were conducted in a similar manner as described on topic 2.2, with a total length of 300 minutes or until the entire solution in T1 was processed, whichever occurred first. But for the continuous system, a sample was collected at the conclusion of each experiment to ascertain the concentration of 4-chlorophenol (4CP). This concentration was then utilized in Equation 2 to calculate the degradation efficiency, adhering to the same structure outlined in Equation 1 [34]:

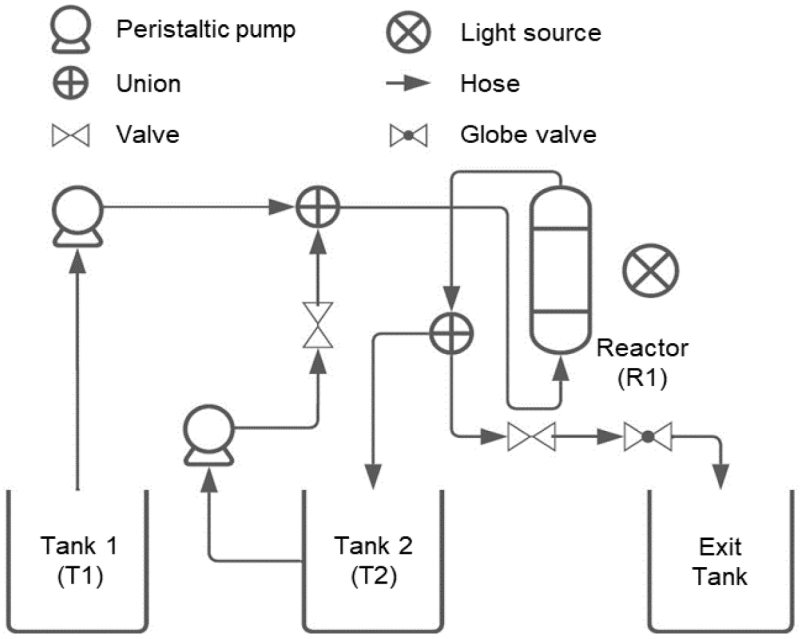

Fig. 1. Fluidized bed reactor system.

$$Degradation\ (\%): \frac{[4CP]_{fresh\ feed}\ (mg\ L^{-1}) - [4CP]_{exit\ tank}\ (mg\ L^{-1})}{[4CP]_{fresh\ feed}\ (mg\ L^{-1})} \times 100 \quad (2)$$

Initially, the effect of the fresh inlet flow rate on the efficiency of the photodegradation process was studied. To do so, the fresh inlet flow rate was varied from 0.07 to 0.33 L h^{-1}, and the recycle flow rate was maintained at 35 L h^{-1}. After determining the optimal fresh inlet flow, the effect of the recycling rate on the efficiency of the photodegradation process was studied. For this purpose, the previously determined optimal fresh inlet flow rate was maintained, while the recycle flow rate was varied from 10 to 35 L h^{-1}.

2.5. Reaction kinetics via computational methods

To achieve a better understanding of the behavior of the photocatalyst (ZnO/g-C_3N_4/carbon xerogel) particles in the continuous reaction system, as well as to determine the reaction kinetics of the degradation process, mathematical modeling was conducted, aiming to propose possible models that could govern the system.

For this purpose, the reaction A→P was considered, with an assumed order of 1, based on recent results obtained by our research group [22]. Moreover, the parameters used for the modeling and simulation were the same as described for the experimental portion of this study, aforementioned in the topic 2.4. Additionally, the integrated equation for the molar balance of the fluidized bed reactor discussed here, starting from the power law [36], is shown below in Equation 3:

$$X_A = 1 - exp(-k\tau) \quad (3)$$

However, the reactor is fed with two streams containing compound A, as shown in Equation 4:

$$F_{A_1} = F_{A_0} + F_{A_R} \quad (4)$$

Equations 5-8 represent the calculations of the variables from Equation 4:

$$F_{A_0} = C_{A_0} v_0 \quad (5)$$

$$v_1 = v_0 + v_R \quad (6)$$

$$\tau = \frac{V}{v_1} \quad (7)$$

$$F_{A_R} = C_{A_R} v_R \quad (8)$$

The molar flow rate of A at the reactor outlet is calculated as follows (Equation 9):

$$F_{A_2} = F_{A_1}(1 - X_A) \quad (9)$$

The balance equations in the recycle and exit tanks are Equations 10 and (11):

$$\frac{dN_{A_R}}{dt} = F_{A_{iR}} - F_{A_R} \quad (10)$$

$$\frac{dN_{A_e}}{dt} = F_{A_e} \quad (11)$$

Where the variables can be calculated as shown in Equations 12-14:

$$F_{A_{iR}} = v_R C_{A_2} \quad (12)$$

$$C_{A_2} = \frac{F_{A_2}}{v_1} \quad (13)$$

$$F_{A_e} = v_0 C_{A_2} \quad (14)$$

The overall conversion (Equation 15) can be calculated in the same manner as discussed for Equation 2:

$$X_{A_g} = \frac{(C_{A_0} - C_{A_e})}{C_{A_0}} \quad (15)$$

Where the variables can be calculated as shown in Equations 16-17:

$$C_{A_e} = \frac{N_{A_e}}{V_e} \quad (16)$$

$$V_e = v_0 t \quad (17)$$

With the molar balance equations obtained, some situations were considered for the investigation of the reaction kinetics based on experimentally obtained data for optimizing the fresh inlet flow rate (F_{A_0}):

1. The whole catalyst returns to the recycle tank (an ideal situation where there is no loss of catalyst at the system's outlet).
2. The catalyst at the reactor outlet is divided into the outlet and recycle tanks at a ratio that is practically equal to the recycle ratio (as shown in Equation 18).

$$C_{C_R} = 0.99 C_C \frac{v_R}{v_1} \tag{18}$$

The difference between the two cases is that in the first case, the obtained k is a constant (comprising the constant catalyst concentration), and, in the second case, there is a dependency of k on the catalyst concentration, i.e., a second order reaction is considered: first order for the pollutant and first order for the catalyst.

The system of equations obtained was solved for each case using the well-known ordinary differential equation numerical integration algorithm, in SciLab version 6.0.0 software [29–31]. The predicted data obtained were compared with experimental data obtained at different fresh inlet flows (with the recycle fixed at 35 L.h^{-1}), aiming to find the best correlation between the two tested cases (i.e., the highest R^2).

With the best-case defined, simulations were conducted based on it for further development of a model to better describe the system. At this stage, experimental data obtained during the optimization of the best recycle flow rate were used (with the fresh inlet flow fixed at the previously optimized value of 0.07 L h^{-1}) as basis for the comparison with the predicted data to be obtained.

3. Results and discussions

3.1. Photocatalytic properties and mechanism evaluation

Fig. 2 depicts the photodegradation results of 4CP using the ZnO/g-C_3N_4/carbon xerogel, the binary systems ZnO/g-C_3N_4 and ZnO/carbon xerogel, and the unary systems ZnO and g-C_3N_4 in a jacketed batch reactor under visible radiation. It is possible to acknowledge that g-C_3N_4 presented the worst degradation results for 4CP, which was already expected, due to its high recombination rates [17,37,38]. ZnO, in turn, exhibited higher photocatalytic efficiency compared to g-C_3N_4, despite its known low absorption of visible light and high recombination rate [14–16,39]. This result can be explained by the presence of oxygen vacancies, leading to the creation of an isolated defect state below the conduction band of ZnO, which likely contributes to higher activity under visible radiation [40,41].

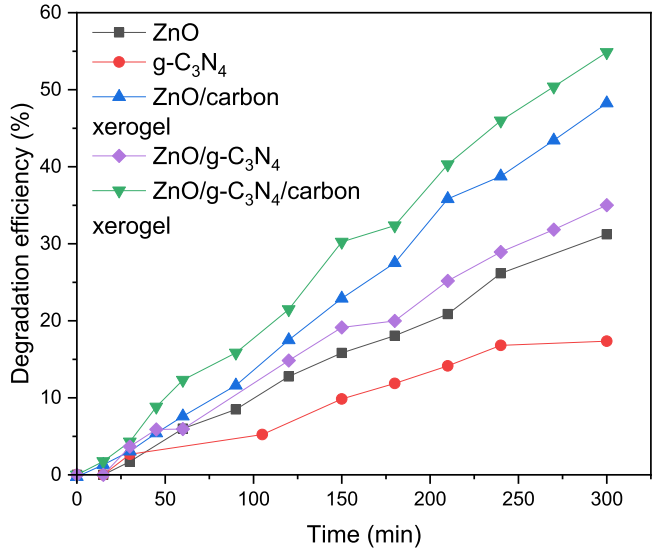

Fig. 2. Photodegradation of 4CP under visible radiation in a batch jacketed reactor using ternary, binary, and unary semiconductors.

However, when comparing pure ZnO with ZnO/g-C_3N_4, the binary system exhibited better efficiency, likely explained by the decrease in the recombination rate induced by the formation of the heterojunction between the semiconductors. The ZnO/carbon xerogel binary system also demonstrated improved efficiency compared to pure ZnO, indicating that the choice of carbon xerogel for the construction of the system is a promising alternative to improve photocatalytic efficiency. This behavior can be explained primarily due to its visible-light sensitization capacity, high specific surface area, and electron sink effect [33].

Moreover, it can be noted the best efficiency results were achieved by the ZnO/g-C_3N_4/carbon xerogel photocatalyst, with a final 4CP degradation percentage of 54.86% after 300 minutes. This outcome can be attributed to the enhanced efficiency of charge transfer and the diminished recombination rate of the electron/hole pairs, resulting from the synergistic effect of the heterojunctions formed within the composite.

Subsequently, electrochemical impedance spectroscopy analysis was conducted to better understand the charge transfer behavior among the tested materials. As shown in Fig. 3A, it can be observed that the test utilizing the ZnO/g-C_3N_4/carbon xerogel ternary exhibited the smallest arc radius, indicating lower resistance to charge transfer under visible light, which can be correlated with the enhanced separation of photogenerated charges and improved photodegradation efficiency, thus demonstrating the positive effect of the heterojunctions formed in the system [42,43]. The results of the other materials also align with the efficiencies observed in the photodegradation of 4-chlorophenol under visible radiation displayed in Fig. 2.

Fig. 3B displays the diffuse reflectance spectra for the tested materials. The ZnO/g-C_3N_4/carbon xerogel and ZnO/carbon xerogel absorb radiation over a broader range than ZnO and g-C_3N_4 and ZnO/g-C_3N_4, which highlights the beneficial effect of the carbon xerogel on the optical properties of the developed materials [22,33,44]. Additionally, pure ZnO shows a small range of visible light absorption between 400 and 450 nm, which aligns with what has been observed and discussed regarding its degradation efficiency under visible light. For the calculation of bandgap energy, a methodology proposed by Ghobadi (2013) [45] was employed, resulting in bandgaps of 3.24 eV, 3.24 eV, 3.19 eV, 3.22 eV and 3.02 for ZnO/g-C_3N_4/carbon xerogel, ZnO/carbon xerogel, ZnO/g-C_3N_4, ZnO and g-C_3N_4, respectively. All materials containing zinc oxide exhibit a comparable bandgap, consistent with literature findings (3.2 eV [46]). The pure g-C_3N_4 similarly aligns with literature-reported values, with a documented bandgap of 3.0 eV [47].

Furthermore, these data were employed to determine the energy levels of the valence and conduction bands of g-C_3N_4 and ZnO, in order to better analyze the charge separation mechanism at the heterojunction formed in the ternary system. For this purpose, Equations 19 and 20 were utilized [12,33,39,48]:

$$E_{CB} = X - E^e - 0.5E_g \tag{19}$$

$$E_{VB} = E_{CB} + E_g \tag{20}$$

where X is the electronegativity of each material ($X_{g\text{-}C3N4} = 4.72$ eV and $X_{ZnO} = 5.75$ eV) [33,49], E_{CB} and E_{VB} correspond to the energies in the conduction and valence bands of each material, and E^e is the energy of free electrons vs. hydrogen ($E^e = 4.5$ eV) [33]. The results obtained for the band energies in the unary systems are shown in Table 1.

After determining the best material for the degradation of 4CP, understanding its charge transfer behavior and finding its band structure, the ZnO/g-C_3N_4/carbon xerogel was subjected to a test in the same jacketed batch reactor system previously utilized, but under solar radiation. From Fig. 4, it is possible to observe that the degradation efficiency under solar radiation showed a better response compared to the results under visible radiation after 300 minutes, with degradation

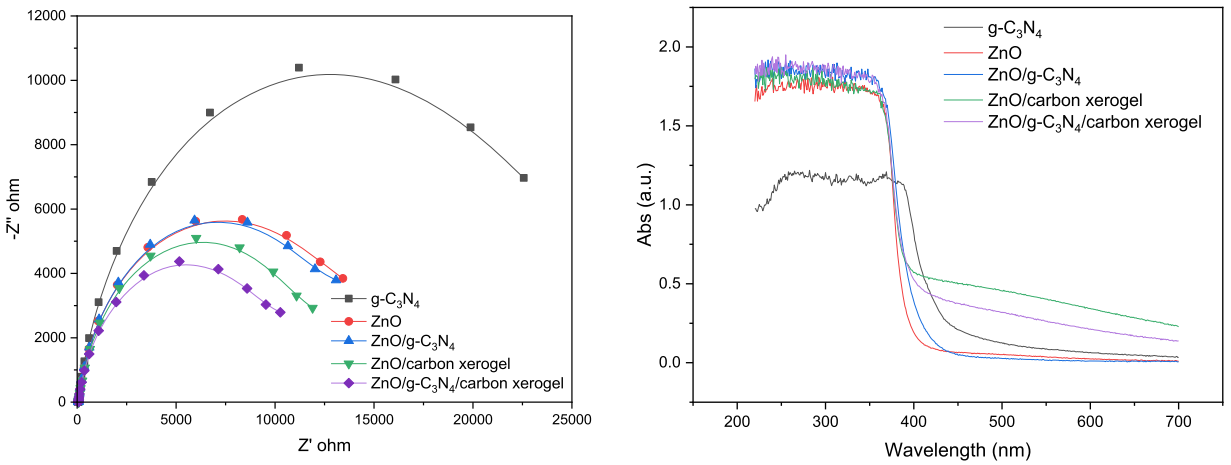

Fig. 3. A) Electrochemical impedance spectroscopy tests under visible radiation; B) Diffuse reflectance spectra for ZnO/g-C_3N_4/carbon xerogel, ZnO/carbon xerogel, g-C_3N_4 and ZnO.

Table 1
Band energy values for the unary materials

Material	E_{CB} (eV)	E_{VB} (eV)
g-C_3N_4	-1.29	1.73
ZnO	-0.36	2.86

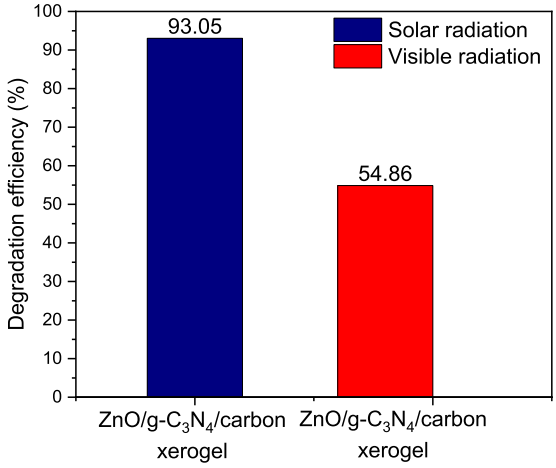

Fig. 4. Comparative study of the final degradations obtained from the ternary material for different light radiations in the jacketed batch reactor.

percentages of 93.05% and 54.86%, respectively. This is explained by the presence of ultraviolet light in the spectrum of the simulated sunlight, as this type of radiation is known to lead to a facilitated photoexcitation process due to its higher energy [33].

Following the simulated solar radiation tests, analyses were conducted to propose a possible mechanism for active radical generation involved in the system. Fig. 5 shows the tests with scavenging agents, which depict that hydroxyl radicals have the greatest influence on the reaction, since with the addition of isopropanol, there was a decrease in the photodegradation efficiency of 4CP with the ternary material from 67% to 13%. However, electrons and superoxide radicals also demonstrate a significant effect on degradation efficiency, while the suppression of vacancies exhibits the least intense effect. A potential mechanism proposed for the formation of active radicals in the system is described in Equations 21-27 [40,50,51].

$$Photocatalyst + \lambda \rightarrow e^- + h^+ \quad (21)$$

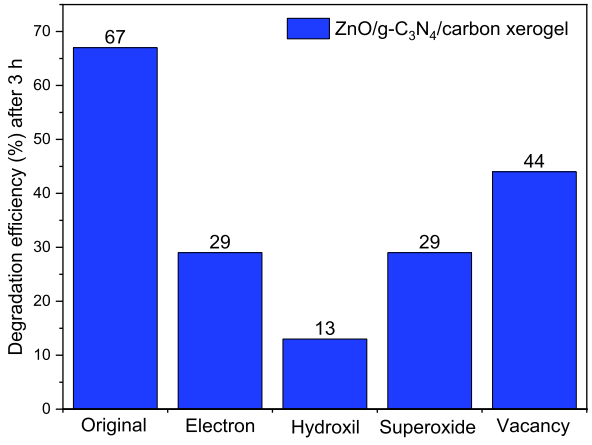

Fig. 5. Evaluation of the effect of adding suppressors for active radicals on the photocatalytic activity of 4CP using ZnO/g-C_3N_4/carbon xerogel in a batch jacketed reactor under solar radiation.

$$H_2O + h^+ \rightarrow \cdot OH + H^+ \quad (22)$$

$$O_2 + e^- \rightarrow O_2^{\cdot -} \quad (23)$$

$$\cdot OH + \cdot OH \rightarrow H_2O_2 \quad (24)$$

$$e^- + O_2^{\cdot -} + 2H^+ \rightarrow H_2O_2 \quad (25)$$

$$e^- + H_2O_2 \rightarrow \cdot OH + OH^- \quad (26)$$

$$H_2O_2 + O_2^{\cdot -} \rightarrow \cdot OH + O_2 + OH^- \quad (27)$$

The influence of the route depicted in Equation 22 can be readily understood through the dependence of degradation efficiency on the presence of hydroxyl radicals (degrading the pollutant). However, as the suppression of electrons and superoxides yielded similar results in terms of photodegradation efficiency, it is possible to assert that the reduction pathway of adsorbed oxygen Equation 23) also plays a role in the reaction, either for the potential degradation of pollutants with the formed superoxide or, more likely, for the generation of hydroxyl radicals from the formed superoxide (Equations 25-(27). Moreover, despite the counterintuitive low effect of vacancies, the result can be explained by the reduction in the recombination of photo-generated charges relative to vacancy suppression, resulting in a higher concentration of electrons in the medium, favoring Equation 23. This can compensate for the lack

of hydroxyl radical generation via Equation 22, as previously mentioned.

Furthermore, using the data from Table 1 and considering a possible direct type-Z heterojunction, the electric field formed between ZnO and g-C_3N_4, due to the proximity of the semiconductors and interaction of the present charges, induces recombination of electrons and vacancies with lower redox abilities (ZnO conduction band = -0.36 eV and g-C_3N_4 valence band = 1.73 eV), thus preserving the photo-generated electrons in the conduction band of g-C_3N_4 (-1.29 eV) and vacancies in the valence band of ZnO (2.86 eV), consistent with the formation of the heterojunction discussed in the results of electrochemical impedance spectroscopy [33,52]. Finally, vacancies in the valence band of ZnO can promote the formation of hydroxyl radicals (E^0 = 2.7 V vs. NHE), and electrons in the conduction band of g-C_3N_4 can promote the reduction of adsorbed oxygen to superoxide (E^0 = -0.285V vs. NHE), in agreement with the results of tests using scavengers discussed earlier [33,53–55].

After determining that ZnO/g-C_3N_4/carbon xerogel is the photocatalyst with the highest photocatalytic efficiency and analyzing its charge transfer behavior, as well as the mechanism of active radical generation, the composite was then thoroughly characterized, followed by the proposed study in the fluidized bed reactor.

3.2. Characterization

The results obtained in the XRD analysis are illustrated in Fig. 6A. In the diffraction pattern of ZnO/g-C_3N_4/carbon xerogel, it is possible to observe peaks at 31.9°, 34.7°, 36.5°, 47.8°, 56.8°, 63°, 66.6°, 68.2°, and 69.2°. The observed peaks are related to the zinc oxide's hexagonal phase (Wurtzite), but with slight shifts, as can be seen from the ZnO (wurtzite) standard data (JCPDS 36-1451). This difference indicates a distortion of the crystal lattice of the material, which can be attributed to the incorporation of carbon atoms into the ZnO's crystalline structure; this result can be explained by the diffusion of carbon through the ZnO's (Wurtzite) structure, caused by the heat treatment to which the samples were subjected [21,56]. Furthermore, Zn-N bonds can be formed from the chemical bonding between the hydroxyl groups of ZnO and the triazine amino group of g-C_3N_4, which can also contribute to the distortion observed in the position of the ternary peaks relative to the standard ZnO, due to the insertion of nitrogen into the ZnO lattice [22,57].

In the IR spectra of ZnO/g-C_3N_4/carbon xerogel and g-C_3N_4 (Fig. 6B), peaks are observed at 810, in the range of 900 to 1700, and broader peaks between 3000 and 3500 cm^{-1}. At 810 cm^{-1}, the peak can be attributed to the characteristic vibration of the tri-s-triazine unit [58], while in the range of 900 to 1700 cm^{-1}, the stretching of vibration signals from the C-N and C=N bonds present in g-C_3N_4 can be observed [59]. The broad peaks close to 3250 cm^{-1} are associated with N-H bonds along with the stretching vibrations of O-H bonds present in water molecules adsorbed on the material's surface [58,59]. ZnO's presence can be confirmed through the appearance of characteristic bands at 700 and 900 cm^{-1}, indicative of the bonds formed between zinc and oxygen, inherent to the ZnO structure [33,60]. Fig. 7A, B show the micrographs obtained for the developed photocatalyst, whereas Fig. 7C, D, E, F, G display the elemental mapping obtained by energy dispersive spectroscopy.

Observing the micrographs of the semiconductor (Fig. 7A, B), it is possible to notice that the ternary compound exhibits nanoscale particles with a shape resembling spheres. This shape may have been inherited from the structure of ZnO, as it has been reported to be composed of nanoscale particles with spherical shapes [21,22].

The results obtained in the elemental mapping of the semiconductor (Fig. 7D, E, F, G) indicate that, for the studied sample, there is a homogeneous distribution of elements on the composite's surface. This distribution can lead to an enhancement in the photocatalytic efficiency of the ternary composite, as it facilitates the charge transfer at the heterojunction between each component, thus promoting the separation of the electron pairs generated through photonic excitation [21].

Raman spectroscopy was performed to corroborate the presence of the semiconductors on the studied composite (ZnO/g-C_3N_4/carbon xerogel). Fig. 8 shows the spectra for the ternary, in which the peaks at 260, 330, 437 and 572 cm^{-1} can respectively be correlated to the B_1 (low) silent mode, E_2 (high) – E_2 (low) mode, E_2 (high) mode [22,61] and A_1 (low) mode for the zinc oxide [22,61]. The wide peak in the spectral range of 1050 to 1200 cm^{-1} is indicative of the acoustic combination of the A1 and E1 modes in zinc oxide [22,62], while the peak at 1380 correspond to the carbon D-band, and, at 1580 cm^{-1}, the peak is attributed to the carbon G-band [63].

3.3. Determination of flow parameters and computational determination of reaction kinetics

3.3.1. Experimental results

Fig. 9 shows the results obtained for the variation of fresh inlet flow rate and recycle rate during the photodegradation tests.

According to Fig. 9A, it was possible to observe that with the variation made in the fresh inlet flow rate of the fluidized reactor for 4CP degradation with solar radiation (whilst keeping the recycle flow rate at 35 L h^{-1}), the system's behavior led to a decrease in the degradation

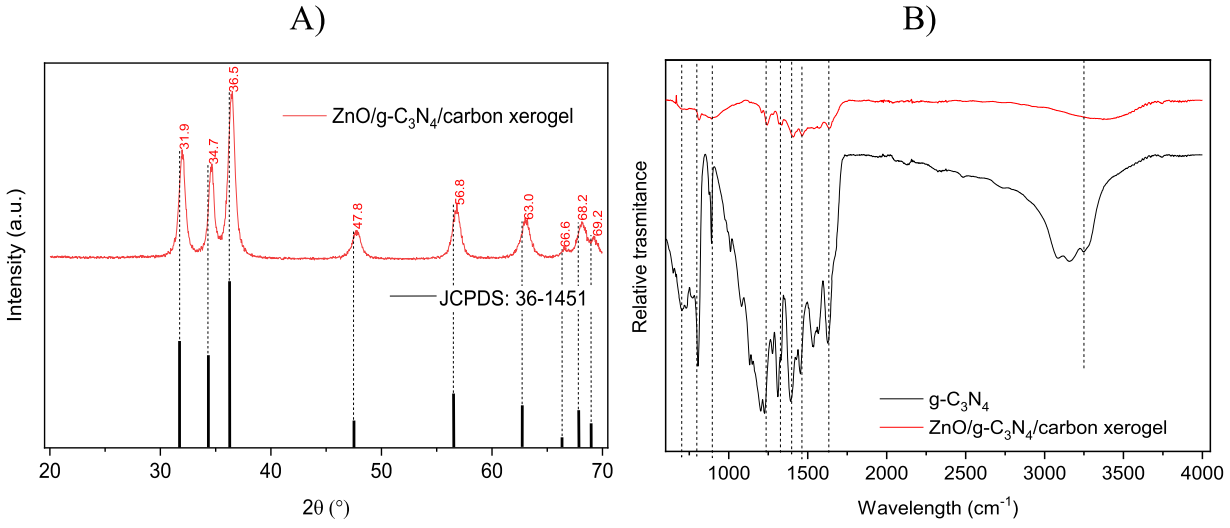

Fig. 6. (A) Diffractogram of the ZnO/g-C_3N_4/carbon xerogel photocatalyst; (B) IR spectra of ZnO/g-C_3N_4/carbon xerogel.

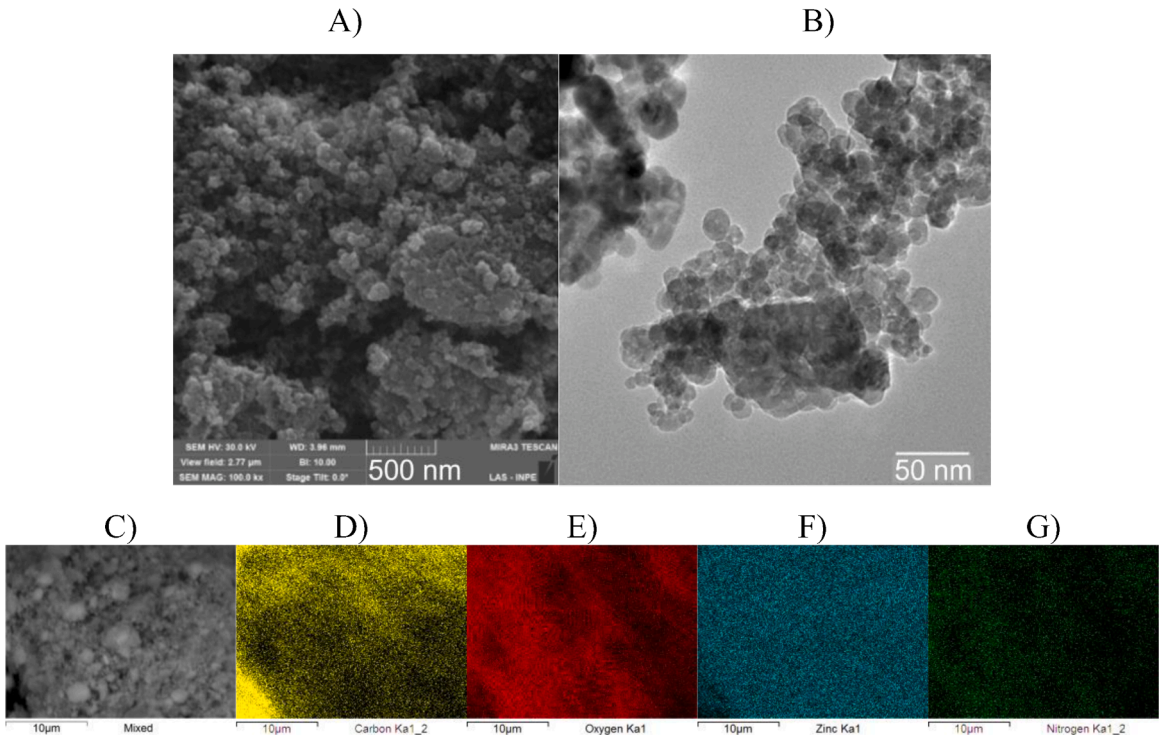

Fig. 7. A) Scanning electron micrograph (50000x) of ZnO/g-C_3N_4/carbon xerogel photocatalyst; B) Transmission electron micrograph (500000x) of the ZnO/g-C_3N_4/carbon xerogel photocatalyst; Elemental mapping of ZnO/g-C_3N_4/carbon xerogel: (C) micrograph, (D) carbon distribution, (E) oxygen distribution, (F) zinc distribution, and (G) nitrogen distribution in the matrix.

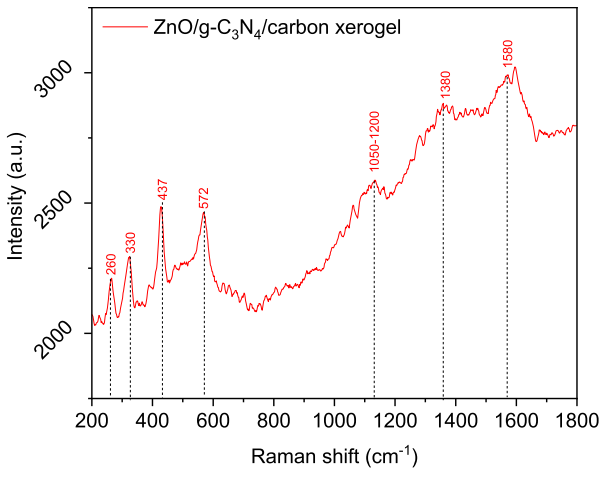

Fig. 8. Raman spectra of ZnO/g-C_3N_4/carbon xerogel.

percentage as the inlet flow rate increased, and the optimum flow rate obtained was at 0.07 L h^{-1}, with a degradation efficiency percentage of 41.21%. These results can be explained by the reduction in the contact time between the catalyst and the pollutant caused by the increase in the inlet flow rate, in line with several studies in the literature [64–66]. This behavior also leads to the conclusion that if lower flow rates were adopted, higher degradation efficiencies would have probably been obtained, however, 0.07 L h^{-1} was the minimum flow rate value that could be sustained by the pump employed in the system.

In determining the ideal recycle rate associated with the highest degree of 4CP degradation, the best fresh inlet flow rate previously stated (0.07 L h^{-1}) was maintained throughout the entire process. Fig. 9B shows that, at a recycling rate of 25 L h^{-1}, the highest efficiency of the photodegradation process was achieved (47.8%). According to Table 2, it is possible to denote that an increase in the recycle flow is directly related to a decrease in the residence time of the reaction mixture and embedded catalyst. This result is in line with the decrease in degradation efficiency found at recycle values greater than 25 L h^{-1}, since free radicals have less time to react with the pollutant [67]. However, for recycle flows less than 25 L h^{-1}, the decrease in degradation efficiency is explained by the lower dispersion of the catalyst obtained, which can lead to greater particle agglomeration and a consequent reduction in degradation efficiency.

3.3.2. *Reaction kinetics via computational simulation*

The modeling of conversion as a function of fresh feed flow rate was studied in two ways as described earlier. In the first scenario, an ideal situation was considered in which the whole catalyst returns to the recycle tank, meaning there is no catalyst loss. In this situation, it was assumed that the degradation reaction profile was first-order, and as a result, a single value of specific rate constant was obtained, $k = 0.494\ h^{-1}$.

In the second situation, the following assumption was made: the catalyst at the reactor outlet is divided between the exit and recycle tanks in a ratio nearly equal to the recycle ratio as described in Equation 18. In this case, the degradation reaction profile was of second order, where the specific reaction rate obtained varies with catalyst concentration as described in Equation 28:

$$k = 5,2C_c\ h^{-1} \tag{28}$$

The results obtained from modeling conversion as a function of fresh feed flow rate are illustrated in Fig. 10A, B, along with their correlation factors. Observing the results, it is possible to verify that the second approach yielded better results, thus demonstrating that there is indeed a catalyst loss in the exit tank.

Starting from the better-suited model (situation 2, $R^2 = 0,910$), two distinct approaches for the specific reaction rate were again considered to further assess the system's behavior:

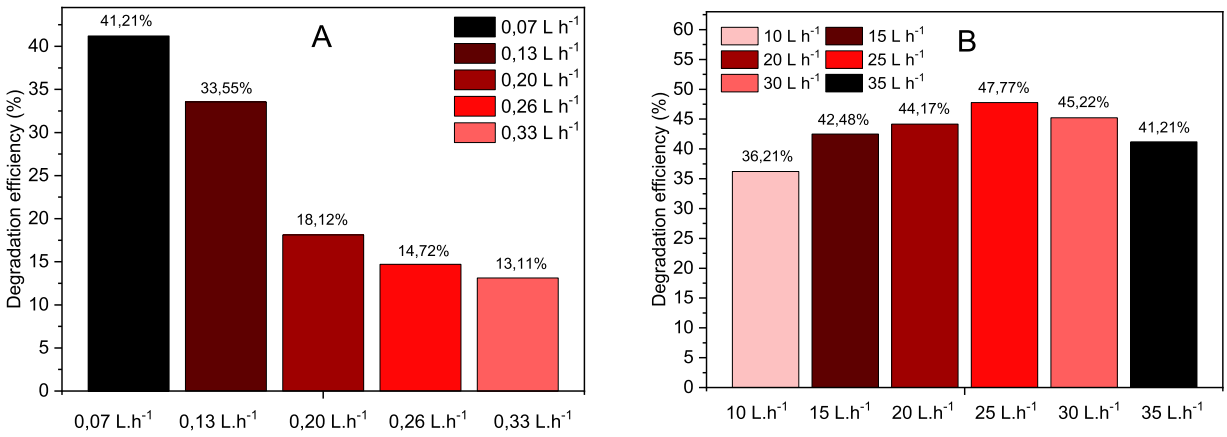

Fig. 9. Optimization of flow parameters in fluidized bed reactor: A) 4CP degradation efficiency by the ternary catalyst at different fresh inlet flow rates; B) 4CP degradation efficiency by the ternary catalyst at different recycle flow rates.

Table 2
Reaction mixture residence time in the fluidized bed reactor for different recycling flows with a fixed value of 0.07 $L.h^{-1}$ for the fresh inlet flow rate

Recycling flow ($L.h^{-1}$)	Reaction mixture residence time ($h.10^{-3}$)
10	14,9
15	9,95
20	7,47
25	5,98
30	4,99
35	4,28

The first approach considers that the parameter k depends on the catalyst concentration in the reactor, as described in Equation 28, and that the catalysis efficiency does not depend on the reactor's feed flow rate.

The second approach also considers that the specific reaction rate depends on the catalyst concentration but assumes that the catalysis efficiency is influenced by the feed flow rate. Therefore, a normal distribution for the catalyst concentration was used. This approach was chosen as it is semi-empirical, allowing for modeling even with a limited amount of data to study the mass transport effects. This distribution considers low efficiency for low flow rates (incapable of dispersing the particles), high efficiency for intermediate flow rates (dispersed particles and low bed porosity), and low efficiency for high flow rates (high bed porosity). The parameter k is given by Equation 29:

$$k = \frac{27}{15\sqrt{2\pi}} exp\left[-\frac{1}{2}\left(\frac{v_R - 25}{15}\right)^2 \right] h^{-1} \quad (29)$$

Analyzing the results presented in Fig. 10C, D, it is possible to see that the second approach yielded better results, thus demonstrating that the catalysis efficiency also depends on the reactor's feed flow rate.

3.4. Photocatalytic efficiency evaluation

Once the optimal fresh inlet feed and recycle flow rates of the reactor were obtained, a study was conducted to assess the ternary's efficiency in degrading the pollutant under both solar and visible radiation in the fluidized bed reactor. The results obtained are illustrated in Fig. 11, and it is evident that the test conducted under solar radiation yielded better results when compared to the tests under visible radiation, similar to what was observed and discussed for the batch reactor tests (Fig. 4).

Upon analyzing the results from Fig. 11 and comparing them with those obtained for the batch system, as shown in Fig. 4, it can be observed that a lower efficiency was achieved for the degradation of 4CP in the continuous system. There was a reduction of 45.28% and 23.88% when shifting from the batch to the continuous system for solar and visible radiation, respectively. This decrease was also noted when comparing the data from Fig. 11 with those obtained in previous work [22], resulting in a decrease of 44.23% (92.00% to 47.77%) and 41.02% (72.00% to 30.98%) when transitioning from the batch to the continuous system for solar and visible radiation, respectively. A recent study showed similar results [68], in which, for the degradation of berberine hydrochloride, the photocatalysts M-TiO_2 (TiO_2 modified with oleic acid) and M-TiO_2/Zr-SiO_2/g-C_3O_4 were used in two systems, batch and continuous, with solar radiation. For both photocatalysts, a decrease in degradation efficiency was observed when transitioning from the batch system to the continuous system (31.52% to 5.79% for M-TiO_2 and 96.85% to 34.83% for M-TiO_2/Zr-SiO_2/g-C_3O_4).

These differences may be linked to the fact that, in continuous reactors, the reactants have shorter residence times relative to the catalyst, which can affect efficiency. Additionally, as previously shown in the modeling and simulation results (topic 3.3.2), there is a loss of catalyst over time. In batch processes, on the other hand, reactants can be kept in contact with the catalyst for longer periods, thereby promoting the reaction [69–71]. Moreover, continuous reactors, even though they exhibit lower efficiency in degradation, still have several advantages compared to batch reactors, among which are reliable scalability, enhanced reaction selectivity, improved reproducibility, rapid mixing, efficient heat exchange and increased safety of operation [25].

4. Conclusion

In conclusion, the ternary material ZnO/g-C_3N_4/carbon xerogel demonstrated superior efficacy compared to its binary and unary counterparts in the photodegradation of 4CP. This superiority can be attributed to its enhanced charge transfer capability, lower recombination rate of electrons and vacancies with higher redox abilities, and broader absorption range under visible radiation. The improved performance is elucidated by the formation of a direct type-Z heterojunction between ZnO/g-C_3N_4 and addition of carbon xerogel to the system. Furthermore, the photodegradation of 4CP exhibited enhanced results under solar radiation in both batch and continuous systems, and the reaction efficacy proved to have high dependence of hydroxyl radicals. The characterizations performed confirmed the presence of the intended components in the ternary and their structural features through the analysis of their crystalline structure, morphology, elemental composition, and chemical structure. Furthermore, the variation in the tested flow parameters for the fluidized bed reactor exerted a substantial impact on the degradation efficiency in the process. In tests related to the variation of the fresh inlet flow rate, the photocatalytic efficiency was inversely proportional to its increase, with the best

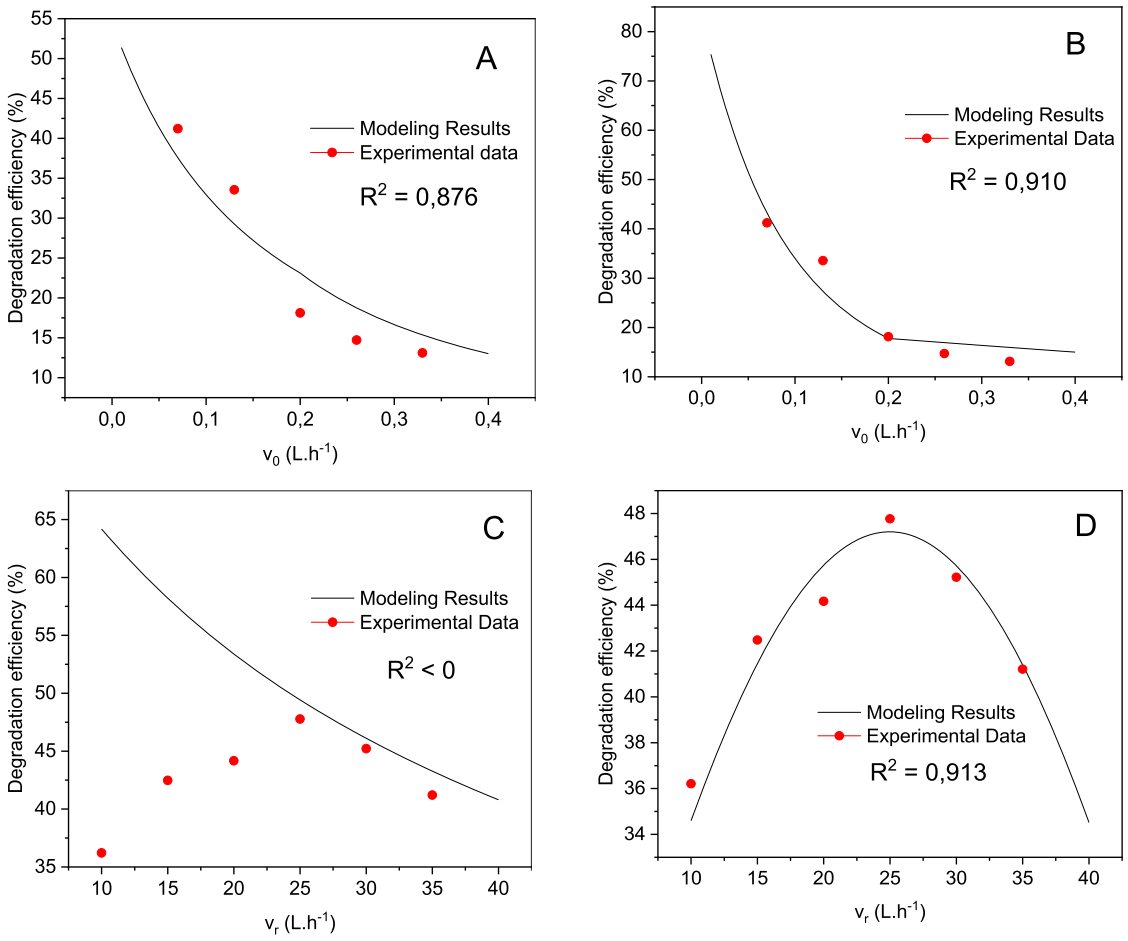

Fig. 10. A) Conversion as a function of fresh inlet flow rate situation 1; B) Conversion as a function of fresh inlet flow rate situation 2; C) Conversion as a function of recycle flow rate situation 1; D) Conversion as a function of recycle flow rate situation.

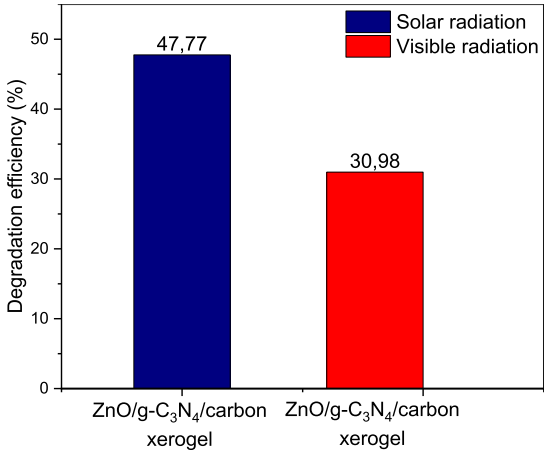

Fig. 11. Comparative study of the final degradations obtained from the ternary material for different light radiations in the fluidized bed reactor.

degradation achieved at the lowest tested value (0.07 L h^{-1}). This conclusion was also observed in the simulation results, which, in addition, showed that there is a dependence of the reaction's specific rate on the concentration of the photocatalyst in the medium. Moreover, for the variation in the recycle flow rate, the best degradation efficiency was obtained at 25 L h^{-1}. In this case, the behavior of the results indicated that both lower and higher flow values negatively affected the degradation efficiency. This aligns with the results of the simulation conducted for this test, which described that the system depends not only on the catalyst concentration but also on how the catalyst efficiency is influenced by the feed flow rate (recycle flow rate representing most of the total reactor inlet flow rate in this study). For recycle flow rates greater than 25 L h^{-1}, the system is affected by the shorter contact time between the catalyst and the reactive medium, while for lower flow rates, the system is affected by the difficulty in dispersing the catalyst in the medium.

CRediT authorship contribution statement

Maira Elizabeth Vicente Gouvea: Formal analysis, Investigation, Methodology, Validation, Visualization, Writing – original draft. **Flávio Henrique Covolam Boldrin:** Formal analysis, Investigation, Methodology, Validation, Visualization, Writing – original draft, Writing – review & editing. **Bruno Henrique Baena da Silva:** Formal analysis, Investigation, Methodology, Validation, Visualization, Writing – original draft. **Livia Kent Paiva:** Formal analysis, Investigation, Methodology, Validation, Visualization, Writing – original draft. **Nicolas Perciani de Moraes:** Formal analysis, Investigation, Methodology, Software, Supervision, Validation, Visualization, Writing – original draft, Writing – review & editing. **Leandro Gonçalves de Aguiar:** Formal analysis, Investigation, Methodology, Software, Supervision, Validation, Visualization, Writing – original draft, Writing – review & editing. **Liana Alvares Rodrigues:** Formal analysis, Funding acquisition, Investigation, Methodology, Project administration, Software, Supervision, Validation, Visualization, Writing – original draft, Writing –

review & editing.

Declaration of Competing Interest

The authors declare that they have no known competing financial interests or personal relationships that could have appeared to influence the work reported in this paper.

Data availability

Data will be made available on request.

Acknowledgments

The authors acknowledge the financial support provided by the São Paulo Research Foundation (FAPESP) (Grants Nº 2018/10492-1, Nº 2018/06361-9 and Nº 2022/04058-2), by the Coordination for the Improvement of Higher Education Personnel Foundation (CAPES) (Processes N° 88887.842112/2023-00 and Nº 88887.829071/2023-00) and by the National Council for Scientific and Technological Development (CNPq) (Grant N° 308576/2022-5). The authors are also grateful to TANAC S.A., which supplied the black wattle tannin (PHENOTAN AP).

References

[1] Y.-C. Nie, F. Yu, L.-C. Wang, Q.-J. Xing, X. Liu, Y. Pei, J.-P. Zou, W.-L. Dai, Y. Li, S. L. Suib, Photocatalytic degradation of organic pollutants coupled with simultaneous photocatalytic H2 evolution over graphene quantum dots/Mn-N-TiO2/g-C3N4 composite catalysts: performance and mechanism, Appl. Catal. B Environ. 227 (2018) 312–321, https://doi.org/10.1016/j.apcatb.2018.01.033.

[2] T. Liu, C.O. Aniagor, M.I. Ejimofor, M.C. Menkiti, K.H.D. Tang, B.L.F. Chin, Y. H. Chan, C.L. Yiin, K.W. Cheah, Y. Ho Chai, S.S.M. Lock, K.L. Yap, M.X.J. Wee, P.-S. Yap, Technologies for removing pharmaceuticals and personal care products (PPCPs) from aqueous solutions: recent advances, performances, challenges and recommendations for improvements, J. Mol. Liq. 374 (2023), 121144, https://doi.org/10.1016/j.molliq.2022.121144.

[3] A.A. Basheer, Chemical chiral pollution: impact on the society and science and need of the regulations in the 21st century, Chirality 30 (2018) 402–406, https://doi.org/10.1002/chir.22808.

[4] M.B. Ahmed, J.L. Zhou, H.H. Ngo, W. Guo, N.S. Thomaidis, J. Xu, Progress in the biological and chemical treatment technologies for emerging contaminant removal from wastewater: a critical review, J. Hazard. Mater. 323 (2017) 274–298, https://doi.org/10.1016/j.jhazmat.2016.04.045.

[5] D. Belhaj, R. Baccar, I. Jaabiri, J. Bouzid, M. Kallel, H. Ayadi, J.L. Zhou, Fate of selected estrogenic hormones in an urban sewage treatment plant in Tunisia (North Africa), Sci. Total Environ. 505 (2015) 154–160, https://doi.org/10.1016/j.scitotenv.2014.10.018.

[6] Z. Yang, X. Zhang, S. Pu, R. Ni, Y. Lin, Y. Liu, Novel Fenton-like system (Mg/Fe-O2) for degradation of 4-chlorophenol, Environ. Pollut. 250 (2019) 906–913, https://doi.org/10.1016/j.envpol.2019.04.096.

[7] J. Zhao, Y. Zhang, X. Quan, S. Chen, Enhanced oxidation of 4-chlorophenol using sulfate radicals generated from zero-valent iron and peroxydisulfate at ambient temperature, Sep. Purif. Technol. 71 (2010) 302–307, https://doi.org/10.1016/j.seppur.2009.12.010.

[8] M. Wang, G. Fang, P. Liu, D. Zhou, C. Ma, D. Zhang, J. Zhan, Fe 3 O 4 @β-CD nanocomposite as heterogeneous Fenton-like catalyst for enhanced degradation of 4-chlorophenol (4-CP), Appl. Catal. B Environ. 188 (2016) 113–122, https://doi.org/10.1016/j.apcatb.2016.01.071.

[9] Y. Hou, X. Li, Q. Zhao, X. Quan, G. Chen, Electrochemically assisted photocatalytic degradation of 4-chlorophenol by ZnFe 2 O 4 −modified TiO 2 nanotube array electrode under visible light irradiation, Environ. Sci. Technol. 44 (2010) 5098–5103, https://doi.org/10.1021/es100004u.

[10] S. Ahmed, F.S.A. Khan, N.M. Mubarak, M. Khalid, Y.H. Tan, S.A. Mazari, R.R. Karri, E.C. Abdullah, Emerging pollutants and their removal using visible-light responsive photocatalysis – a comprehensive review, J. Environ. Chem. Eng. 9 (2021), 106643, https://doi.org/10.1016/j.jece.2021.106643.

[11] M. Hu, P. Zhu, M. Liu, J. Xu, M. Duan, J. Lin, Preparation, performance and mechanism of p-Ag3PO4/n-ZnO/C heterojunction with IRMOF-3 as precursor for efficient photodegradation of norfloxacin, Colloids Surfaces A Physicochem. Eng. Asp. 628 (2021), 127235, https://doi.org/10.1016/j.colsurfa.2021.127235.

[12] P. Zhu, J. Lin, L. Xie, M. Duan, D. Chen, D. Luo, Y. Wu, Visible light response photocatalytic performance of Z-scheme Ag 3 PO 4 /GO/UiO–66–NH 2 photocatalysts for the levofloxacin hydrochloride, Langmuir 37 (2021) 13309–13321, https://doi.org/10.1021/acs.langmuir.1c01901.

[13] A. Mathialagan, M. Manavalan, K. Venkatachalam, F. Mohammad, W.C. Oh, S. Sagadevan, Fabrication and physicochemical characterization of g-C3N4/ZnO composite with enhanced photocatalytic activity under visible light, Opt. Mater. 100 (2020), 109643, https://doi.org/10.1016/j.optmat.2019.109643.

[14] L. Li, S.-Q. Sun, Y.-X. Wang, C.-Y. Wang, Facile synthesis of ZnO/g-C3N4 composites with honeycomb-like structure by H2 bubble templates and their enhanced visible light photocatalytic performance, J. Photochem. Photobiol. A Chem. 355 (2018) 16–24, https://doi.org/10.1016/j.jphotochem.2017.12.016.

[15] L. Liu, X. Luo, Y. Li, F. Xu, Z. Gao, X. Zhang, Y. Song, H. Xu, H. Li, Facile synthesis of few-layer g-C3N4/ZnO composite photocatalyst for enhancing visible light photocatalytic performance of pollutants removal, Colloids Surfaces A Physicochem. Eng. Asp. 537 (2018) 516–523, https://doi.org/10.1016/j.colsurfa.2017.09.051.

[16] N.P. de Moraes, R.B. Valim, R. da Silva Rocha, M.L.C.P. da Silva, T.M.B. Campos, G.P. Thim, L.A. Rodrigues, Effect of synthesis medium on structural and photocatalytic properties of ZnO/carbon xerogel composites for solar and visible light degradation of 4-chlorophenol and bisphenol A, Colloids Surfaces A Physicochem. Eng. Asp. 584 (2020), 124034, https://doi.org/10.1016/j.colsurfa.2019.124034.

[17] P. Zhu, J. Xu, M. Duan, R. Wang, L. Xie, M. Hu, P. Wang, Fabrication of a double Z-type g-C3N4/AgBr/Ag3PO4 composite with enhanced visible-light photocatalytic activity for organic dye elimination, Opt. Mater. 107 (2020), 110076, https://doi.org/10.1016/j.optmat.2020.110076.

[18] P. Zhu, M. Hu, M. Duan, L. Xie, M. Zhao, High visible light response Z-scheme Ag3PO4 /g-C3N4 / ZnO composite photocatalyst for efficient degradation of tetracycline hydrochloride: preparation, properties and mechanism, J. Alloys Compd. 840 (2020), 155714, https://doi.org/10.1016/j.jallcom.2020.155714.

[19] L. Xie, P. Zhu, J. Xu, M. Duan, S. Zhang, X. Wu, Highly Efficient Bi 4 Ti 3 O 12 /g-C 3N 4 /BiOBr dual Z-scheme heterojunction photocatalysts with enhanced visible light-responsive activity for the degradation of antibiotics, Langmuir 38 (2022) 9532–9545, https://doi.org/10.1021/acs.langmuir.2c00907.

[20] P. Zhu, D. Luo, M. Liu, M. Duan, J. Lin, X. Wu, Flower-globular BiOI/BiVO4/g-C3N4 with a dual Z-scheme heterojunction for highly efficient degradation of antibiotics under visible light, Sep. Purif. Technol. 297 (2022), 121503, https://doi.org/10.1016/j.seppur.2022.121503.

[21] N.P. de Moraes, L.A. Bacetto, G.S. dos Santos, M.L.C. Pinto da Silva, J.P. B. Machado, T.M.B. Campos, G.P. Thim, L.A. Rodrigues, Synthesis of novel ZnO/carbon xerogel composites: effect of carbon content and calcination temperature on their structural and photocatalytic properties, Ceram. Int. 45 (2019) 3657–3667, https://doi.org/10.1016/j.ceramint.2018.11.027.

[22] J.G.M. de Sousa, T.V.C. da Silva, N.P. de Moraes, M.L. Caetano Pinto da Silva, R. da Silva Rocha, R. Landers, L.A. Rodrigues, Visible light-driven ZnO/g-C3N4/carbon xerogel ternary photocatalyst with enhanced activity for 4-chlorophenol degradation, Mater. Chem. Phys. 256 (2020), 123651, https://doi.org/10.1016/j.matchemphys.2020.123651.

[23] J.C. Castillo-Rodríguez, F. Tzompantzi, C. Tzompantzi-Flores, M.E. Velásquez-Torres, R. Gómez, C.E. Santolalla-Vargas, M.A. Álvarez Lémus, E. Ramos-Ramírez, G. Del Ángel Montes, High photoactivity of ZrxOy-Bi2O2(CO3) composite materials prepared by one-step synthesis for efficient photodegradation of 4-chlorophenol in water, J. Photochem. Photobiol. A Chem. 435 (2023), 114285, https://doi.org/10.1016/j.jphotochem.2022.114285.

[24] N.P. de Moraes, L.G.P. Marins, M.Y. de Moura Yamanaka, R. Bacani, R. da Silva Rocha, L.A. Rodrigues, Efficient photodegradation of 4-chlorophenol under solar radiation using a new ZnO/ZnS/carbon xerogel composite as a photocatalyst, J. Photochem. Photobiol. A Chem. 418 (2021), 113377, https://doi.org/10.1016/j.jphotochem.2021.113377.

[25] D. Cambié, C. Bottecchia, N.J.W. Straathof, V. Hessel, T. Noël, Applications of continuous-flow photochemistry in organic synthesis, material science, and water treatment, Chem. Rev. 116 (2016) 10276–10341, https://doi.org/10.1021/acs.chemrev.5b00707.

[26] F. Tisa, A.A. Abdul Raman, W.M.A. Wan Daud, Applicability of fluidized bed reactor in recalcitrant compound degradation through advanced oxidation processes: a review, J. Environ. Manage. 146 (2014) 260–275, https://doi.org/10.1016/j.jenvman.2014.07.032.

[27] G. Moussavi, A.A. Aghapour, K. Yaghmaeian, The degradation and mineralization of catechol using ozonation catalyzed with MgO/GAC composite in a fluidized bed reactor, Chem. Eng. J. 249 (2014) 302–310, https://doi.org/10.1016/j.cej.2014.03.059.

[28] G.J. Rincón, E.J. La Motta, A fluidized-bed reactor for the photocatalytic mineralization of phenol on TiO2-coated silica gel, Heliyon 5 (2019) e01966, https://doi.org/10.1016/j.heliyon.2019.e01966.

[29] N.M.L. Nohara, H.J. Izário Filho, A.F. Siqueira, L.G. de Aguiar, G.C.K. de Oliveira, E.L. Nohara, M.A.K. de Alcântara, D.A. dos S. Napoleão, Study of the effectiveness of a ZnO–TiO2 formulation in the degradation of humic substances in mature leachate by solar photocatalysis Brazil, Ambient. e Agua - Interdiscip. J. Appl. Sci. 18 (2023) 1–18, https://doi.org/10.21203/rs.3.rs-2294636/v1.

[30] G.H. Enokihara, C.C.A. Loures, H.J. Izário Filho, M.A.K. Alcântara, A.F. Siqueira, P. C.M. Da Rós, D.A.S. Napoleão, L.G. de Aguiar, Kinetic modelling of total organic carbon degradation in dairy wastewater, Environ. Technol. (2022) 1–8, https://doi.org/10.1080/09593330.2022.2130103.

[31] D.A. dos S. Napoleão, H.J. Izário Filho, A.F. Siqueira, E.H. Bredda, L.G. de Aguiar, P.C.M. Da Rós, M.A.K. de Alcântara, Comparative study of data analysis techniques for photo-Fenton degradation of landfill leachate, Ind. Eng. Chem. Res. 61 (2022) 1985–1993, https://doi.org/10.1021/acs.iecr.1c04087.

[32] P. Soriano-Molina, J.L. García Sánchez, O.M. Alfano, L.O. Conte, S. Malato, J. A. Sánchez Pérez, Mechanistic modeling of solar photo-Fenton process with Fe3+-EDDS at neutral pH, Appl. Catal. B Environ. 233 (2018) 234–242, https://doi.org/10.1016/j.apcatb.2018.04.005.

[33] N.P. de Moraes, M.B. de C. Sanmartin, R. da Silva Rocha, A. de Siervo, M.R. de Vasconcelos Lanza, D.A. Reddy, L. Yu, L.A. Rodrigues, ZnO/CeO2/carbon xerogel composites with direct Z-scheme heterojunctions: enhancing photocatalytic remediation of 4-chlorophenol under visible light, J. Rare Earths (2022), https://doi.org/10.1016/j.jre.2022.11.001.
[34] S.C. Yan, Z.S. Li, Z.G. Zou, Photodegradation of rhodamine B and methyl orange over boron-doped g-C 3N4 under visible light irradiation, Langmuir 26 (2010) 3894–3901, https://doi.org/10.1021/la904023j.
[35] N.P. de Moraes, L.H.A. Roupinha, G.S. dos Santos, B.R.C. de Menezes, J.G.M. de Sousa, G.V.J. Dantas, L. Chaguri, L.A. Rodrigues, Synthesis, characterization and application of Nb2O5-doped zinc oxide for solar-based photodegradation of 4-chlorophenol, Mater. Lett. 275 (2020), 128156, https://doi.org/10.1016/j.matlet.2020.128156.
[36] H. Assadi, F. Armaghan, R.A. Taheri, Photocatalytic oxidation of ketone group volatile organic compounds in an intensified fluidized bed reactor using nano-TiO2/UV process: an experimental and modeling study, Chem. Eng. Process. - Process Intensif. 161 (2021), 108312, https://doi.org/10.1016/j.cep.2021.108312.
[37] P. Qiu, C. Xu, H. Chen, F. Jiang, X. Wang, R. Lu, X. Zhang, One step synthesis of oxygen doped porous graphitic carbon nitride with remarkable improvement of photo-oxidation activity: role of oxygen on visible light photocatalytic activity, Appl. Catal. B Environ. 206 (2017) 319–327, https://doi.org/10.1016/j.apcatb.2017.01.058.
[38] X. Miao, X. Yue, Z. Ji, X. Shen, H. Zhou, M. Liu, K. Xu, J. Zhu, G. Zhu, L. Kong, S. A. Shah, Nitrogen-doped carbon dots decorated on g-C3N4/Ag3PO4 photocatalyst with improved visible light photocatalytic activity and mechanism insight, Appl. Catal. B Environ. 227 (2018) 459–469, https://doi.org/10.1016/j.apcatb.2018.01.057.
[39] P. Zhu, M. Duan, R. Wang, J. Xu, P. Zou, H. Jia, Facile synthesis of ZnO/GO/Ag3PO4 heterojunction photocatalyst with excellent photodegradation activity for tetracycline hydrochloride under visible light, Colloids Surfaces A Physicochem. Eng. Asp. 602 (2020), 125118, https://doi.org/10.1016/j.colsurfa.2020.125118.
[40] N.P. de Moraes, R. da Silva Rocha, A. de Siervo, C.C.A. do Prado, T.C.B. de Paiva, T. M.B. Campos, G.P. Thim, M.R. de Vasconcelos Lanza, L.A. Rodrigues, Resorcinol-based carbon xerogel/ZnO composite for solar-light-induced photodegradation of sulfamerazine, Opt. Mater. 128 (2022), 112470, https://doi.org/10.1016/j.optmat.2022.112470.
[41] J. Wang, Y. Xia, Y. Dong, R. Chen, L. Xiang, S. Komarneni, Defect-rich ZnO nanosheets of high surface area as an efficient visible-light photocatalyst, Appl. Catal. B Environ. 192 (2016) 8–16, https://doi.org/10.1016/j.apcatb.2016.03.040.
[42] C. Jin, K. Su, L. Tan, X. Liu, Z. Cui, X. Yang, Z. Li, Y. Liang, S. Zhu, K.W.K. Yeung, S. Wu, Near-infrared light photocatalysis and photothermy of carbon quantum dots and au nanoparticles loaded titania nanotube array, Mater. Des. 177 (2019), 107845, https://doi.org/10.1016/j.matdes.2019.107845.
[43] N.P. de Moraes, F.A. Torezin, G.V. Jucá Dantas, J.G.M. de Sousa, R.B. Valim, R. da Silva Rocha, R. Landers, M.L.C.P. da Silva, L.A. Rodrigues, TiO2/Nb2O5/carbon xerogel ternary photocatalyst for efficient degradation of 4-chlorophenol under solar light irradiation, Ceram. Int. 46 (2020) 14505–14515, https://doi.org/10.1016/j.ceramint.2020.02.249.
[44] N.P. de Moraes, M.L.C.P. da Silva, T.M.B. Campos, G.P. Thim, L.A. Rodrigues, Novel synthetic route for low-cost carbon-modified TiO2 with enhanced visible light photocatalytic activity: carbon content and calcination effects, J. Sol-Gel Sci. Technol. 87 (2018) 380–390, https://doi.org/10.1007/s10971-018-4700-4.
[45] N. Ghobadi, Band gap determination using absorption spectrum fitting procedure, Int. Nano Lett. 3 (2013) 2, https://doi.org/10.1186/2228-5326-3-2.
[46] M.L. Maya-Treviño, M. Villanueva-Rodríguez, J.L. Guzmán-Mar, L. Hinojosa-Reyes, A. Hernández-Ramírez, Comparison of the solar photocatalytic activity of ZnO-Fe2O3 and ZnO-Fe0 on 2,4-D degradation in a CPC reactor, Photochem. Photobiol. Sci. 14 (2015) 543–549, https://doi.org/10.1039/c4pp00274a.
[47] H. Li, Z. Zhang, Y. Liu, W. Cen, X. Luo, Functional group effects on the HOMO–LUMO gap of g-C3N4, Nanomaterials 8 (2018) 589, https://doi.org/10.3390/nano8080589.
[48] P. Singh, A. Sudhaik, P. Raizada, P. Shandilya, R. Sharma, A. Hosseini-Bandegharaei, Photocatalytic performance and quick recovery of BiOI/Fe3O4@graphene oxide ternary photocatalyst for photodegradation of 2,4-dintirophenol under visible light, Mater. Today Chem. 12 (2019) 85–95, https://doi.org/10.1016/j.mtchem.2018.12.006.
[49] A. Masoud, M.A. Ahmed, F. Kühn, G. Bassioni, Nanosheet g-C3N4 enhanced by Bi2MoO6 for highly efficient photocatalyst toward photodegradation of Rhodamine-B dye, Heliyon (2023) e22342, https://doi.org/10.1016/j.heliyon.2023.e22342.
[50] Y. Nosaka, A.Y. Nosaka, Generation and detection of reactive oxygen species in photocatalysis, Chem. Rev. 117 (2017) 11302–11336, https://doi.org/10.1021/acs.chemrev.7b00161.
[51] J. Zhang, Y. Nosaka, Mechanism of the OH radical generation in photocatalysis with TiO 2 of different crystalline types, J. Phys. Chem. C 118 (2014) 10824–10832, https://doi.org/10.1021/jp501214m.
[52] Y. Yuan, R. Guo, L. Hong, X. Ji, Z. Lin, Z. Li, W. Pan, A review of metal oxide-based Z-scheme heterojunction photocatalysts: actualities and developments, Mater. Today Energy 21 (2021), 100829, https://doi.org/10.1016/j.mtener.2021.100829.
[53] N.P. de Moraes, T.M.B. Campos, G.P. Thim, A. de Siervo, M.R. de V. Lanza, L. A. Rodrigues, Application of a new lignin/cellulose carbon xerogel/ZnO/Bi2O3/Bi° composite photocatalyst for the degradation of bisphenol-a under sunlight, Chem. Phys. Impact. 6 (2023), 100182, https://doi.org/10.1016/j.chphi.2023.100182.
[54] S. Yi, X. Yue, D. Xu, Z. Liu, F. Zhao, D. Wang, Y. Lin, Study on photogenerated charge transfer properties and enhanced visible-light photocatalytic activity of p-type Bi 2 O 3 /n-type ZnO heterojunctions, New J. Chem. 39 (2015) 2917–2924, https://doi.org/10.1039/C4NJ01738B.
[55] B.G. Kwon, J. Yoon, Superoxide anion radical: principle and application, J. Korean Ind. Eng. Chem. 20 (2009) 593–602.
[56] R. Taziwa, E. Meyer, D. Katwire, L. Ntozakhe, Influence of carbon modification on the morphological, structural, and optical properties of zinc oxide nanoparticles synthesized by pneumatic spray pyrolysis technique, J. Nanomater. 2017 (2017) 1–11, https://doi.org/10.1155/2017/9095301.
[57] J.-X. Sun, Y.-P. Yuan, L.-G. Qiu, X. Jiang, A.-J. Xie, Y.-H. Shen, J.-F. Zhu, Fabrication of composite photocatalyst g-C3N4–ZnO and enhancement of photocatalytic activity under visible light, Dalt. Trans. 41 (2012) 6756, https://doi.org/10.1039/c2dt12474b.
[58] X. Ou, P. Chen, K. Zhao, C. Xia, Fabrication of Z-scheme ZnO/g-C3N4 heterojunction modified by silver nanoparticles for photocatalytic removal of norfloxacin and rhodamine B, Opt. Mater. 144 (2023), 114305, https://doi.org/10.1016/j.optmat.2023.114305.
[59] H. Zou, X. Yan, J. Ren, X. Wu, Y. Dai, D. Sha, J. Pan, J. Liu, Photocatalytic activity enhancement of modified g-C3N4 by ionothermal copolymerization, J. Mater. 1 (2015) 340–347, https://doi.org/10.1016/j.jmat.2015.10.004.
[60] N. Qin, Q. Xiang, H. Zhao, J. Zhang, J. Xu, Evolution of ZnO microstructures from hexagonal disk to prismoid, prism and pyramid and their crystal facet-dependent gas sensing properties, CrystEngComm 16 (2014) 7062, https://doi.org/10.1039/C4CE00637B.
[61] R. Cuscó, E. Alarcón-Lladó, J. Ibáñez, L. Artús, J. Jiménez, B. Wang, M.J. Callahan, Temperature dependence of Raman scattering in ZnO, Phys. Rev. B 75 (2007), 165202, https://doi.org/10.1103/PhysRevB.75.165202.
[62] R. Zhang, P.-G. Yin, N. Wang, L. Guo, Photoluminescence and Raman scattering of ZnO nanorods, Solid State Sci. 11 (2009) 865–869, https://doi.org/10.1016/j.solidstatesciences.2008.10.016.
[63] S.K.Das Shilpa, M.A.F. Afzal, S. Srivastava, S. Patil, A. Sharma, Enhanced electrical conductivity of suspended carbon nanofibers: effect of hollow structure and improved graphitization, Carbon N. Y. 108 (2016) 135–145, https://doi.org/10.1016/j.carbon.2016.06.103.
[64] W. Abou Saoud, A.A. Assadi, M. Guiza, A. Bouzaza, W. Aboussaoud, A. Ouederni, I. Soutrel, D. Wolbert, S. Rtimi, Study of synergetic effect, catalytic poisoning and regeneration using dielectric barrier discharge and photocatalysis in a continuous reactor: abatement of pollutants in air mixture system, Appl. Catal. B Environ. 213 (2017) 53–61, https://doi.org/10.1016/j.apcatb.2017.05.012.
[65] Y. Li, J. Chen, J. Liu, M. Ma, W. Chen, L. Li, Activated carbon supported TiO2-photocatalysis doped with Fe ions fo continuous treatment of dye wastewater in a dynamic reactor, J. Environ. Sci. 22 (2010) 1290–1296, https://doi.org/10.1016/S1001-0742(09)60252-7.
[66] O. Sacco, M. Matarangolo, V. Vaiano, G. Libralato, M. Guida, G. Lofrano, M. Carotenuto, Crystal violet and toxicity removal by adsorption and simultaneous photocatalysis in a continuous flow micro-reactor, Sci. Total Environ. 644 (2018) 430–438, https://doi.org/10.1016/j.scitotenv.2018.06.388.
[67] T. Mohapatra, P. Ghosh, Photo-Fenton remediation of textile wastewater in fluidized-bed reactor using modified laterite: hydrodynamic study and effect of operating parameters, Chem. Eng. J. 473 (2023), 145324, https://doi.org/10.1016/j.cej.2023.145324.
[68] Y. Yu, X. Hu, M. Li, J. Fang, C. Leng, X. Zhu, W. Xu, J. Qin, L. Yao, Z. Liu, Z. Fang, Constructing mesoporous Zr-doped SiO2 onto efficient Z-scheme TiO2/g-C3N4 heterojunction for antibiotic degradation via adsorption-photocatalysis and mechanism insight, Environ. Res. 214 (2022), 114189, https://doi.org/10.1016/j.envres.2022.114189.
[69] M. Shen, G. Zhang, J. Liu, Y. Liu, J. Zhai, H. Zhang, H. Yu, Visible-light-driven photodegradation of xanthate in a continuous fixed-bed photoreactor: experimental study and modeling, Chem. Eng. J. 461 (2023), 141833, https://doi.org/10.1016/j.cej.2023.141833.
[70] Y. Serhane, N. Belkessa, A. Bouzaza, D. Wolbert, A.A. Assadi, Continuous air purification by front flow photocatalytic reactor: modelling of the influence of mass transfer step under simulated real conditions, Chemosphere 295 (2022), 133809, https://doi.org/10.1016/j.chemosphere.2022.133809.
[71] S. Sarkar, C. Bhattacharjee, S. Sarkar, Studies on the performance of annular photo reactor (APR) for pharmaceutical wastewater treatment, J. Water Process Eng. 19 (2017) 26–34, https://doi.org/10.1016/j.jwpe.2017.07.006.